THE JOURNAL OF PHYSICAL CHEMISTRY C

Article

Cite This: J. Phys. Chem. C 2017, 121, 22826-22835

pubs.acs.org/JPCC

Interlayer Potential for Homogeneous Graphene and Hexagonal Boron Nitride Systems: Reparametrization for Many-Body Dispersion Effects

Tal Maaravi,[†,#] Itai Leven,[†,#] Ido Azuri,[‡] Leeor Kronik,[‡] and Oded Hod*[,†]

[†]Department of Physical Chemistry, School of Chemistry, The Raymond and Beverly Sackler Faculty of Exact Sciences and The Sackler Center for Computational Molecular and Materials Science, Tel Aviv University, Tel Aviv 6997801, Israel

[‡]Department of Materials and Interfaces, Weizmann Institute of Science, Rehovoth 76100, Israel

Supporting Information

ABSTRACT: A new parametrization of the anisotropic interlayer potential for hexagonal boron nitride (*h*-BN ILP) is presented. The force-field is benchmarked against density functional theory calculations of several dimer systems within the Heyd-Scuseria-Ernzerhof hybrid density functional approximation, corrected for many-body dispersion effects. The latter, more advanced method for treating dispersion, is known to produce binding energies nearly twice as small as those obtained with pairwise correction schemes, used for an earlier ILP parametrization. The new parametrization yields good agreement with the reference calculations to within ∼1 and ∼0.5 meV/atom for binding and sliding energies, respectively. For completeness, we present a complementary parameter set for homogeneous graphitic systems. Together with our previously suggested ILP parametrization for the heterogeneous graphene/*h*-BN junction, this provides a powerful tool for consistent simulation of the structural, mechanical, tribological, and heat transport properties of both homogeneous and heterogeneous layered structures based on graphene and *h*-BN.

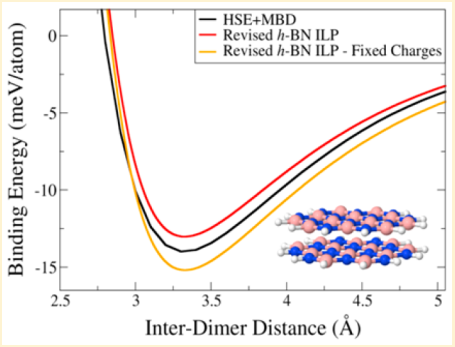

INTRODUCTION

The successful isolation of single layer graphene in 2004[1] has triggered an avalanche of studies aiming to understand the physical and chemical properties of carbon-based and inorganic two-dimensional (2D) layered materials (see, e.g., refs 2−13). The reduced dimensionality of these systems allows for an efficient computational evaluation of their structural and electronic properties within the framework of first-principles calculations based on density functional theory (DFT).[14] Nevertheless, when modeling large nonperiodic structures and their long-term dynamics, DFT becomes prohibitively expensive and one needs to resort to simplified and more computationally efficient approaches.

Classical force-fields (FFs) are one of the most popular alternatives for studying the structural, dynamical, mechanical, tribological, and heat transport characteristics of 2D layered materials. Due to the inherent anisotropy of these systems, FFs are often designed to describe their intra- and interlayer interactions separately. To treat the former, many intralayer FFs have been presented over the years for a variety of material compositions.[15−38] These often include bonded interactions describing two-body bond stretching and compression, three-body bond angle bending, and four-body torsional angle deformations, as well as nonbonded two-body dispersive and electrostatic interactions. The corresponding force-constants and equilibrium values are either empirically fitted or parametrized against higher-accuracy computational methods. As for the interlayer interactions, classical electrostatic Coulomb terms are used whenever significant partial atomic charges exist. These are often augmented by Lennard-Jones or Morse-type potentials to treat the long-range attractive dispersion interactions and the short-range Pauli-repulsions.[22,24,39,40] The latter, however, depend on two-body interatomic distances and therefore fail to capture the anisotropic nature of the layered structure, resulting in too shallow interlayer sliding energy landscapes.[41] This strongly hinders their ability to describe interlayer mechanical and tribological properties.[42]

To address this problem, Kolmogorov and Crespi (KC) presented an anisotropic two-body interlayer potential (ILP) term that depends not only on the interatomic distance but also on interatomic relative lateral displacement.[43,44] The KC-ILP expression consists of a long-range isotropic Lennard-Jones attraction term and a short-range isotropic Morse-like repulsive term, corrected for anisotropic effects by a lateral Gaussian-type repulsion with the following form:

$$V^{\mathrm{KC}}(r_{ij}, \rho_{ij}) = \mathrm{e}^{-\lambda(r_{ij}-z_0)}[C + f(\rho_{ij}) + f(\rho_{ji})] - A(r_{ij}/z_0)^{-6} \quad (1)$$

where $f(\rho) = \mathrm{e}^{-(\rho/\delta)^2}\sum_{n=0}^{2} c_{2n}(\rho/\delta)^{2n}$, λ, z_0, C, A, δ, and c_{2n} are fitting parameters, and r_{ij} and ρ_{ij} are the full and lateral

Received: July 18, 2017
Revised: September 14, 2017
Published: September 18, 2017

DOI: 10.1021/acs.jpcc.7b07091
J. Phys. Chem. C 2017, 121, 22826−22835

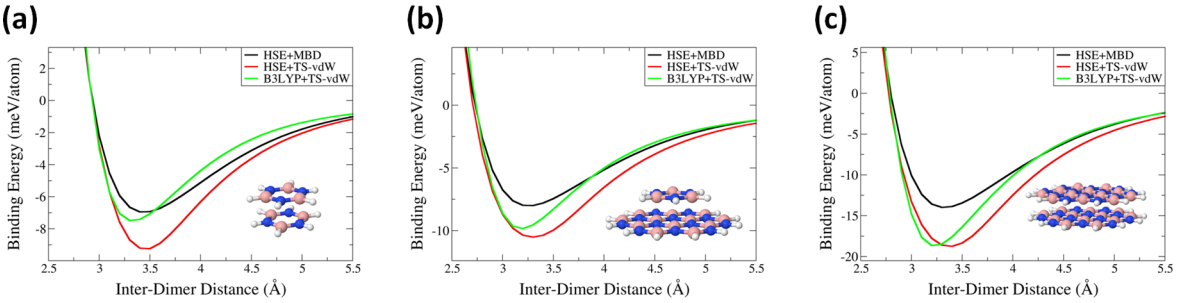

Figure 1. Binding energy curves of (a) the borazine dimer; (b) the borazine/HBNC system; and (c) the HBNC dimer calculated using HSE+MBD (black) compared to HSE+TS-vdW data (red) and to the B3LYP+TS-vdW results of ref 47 (green). The energy axis origin of each curve is set as the energy of the corresponding dimer at a separation of 100 Å.

Table 1. List of ILP Parameter Values for Homogeneous *h*-BN Based Systems, Fitted Against MBD-Corrected DFT Reference Data, Using Variable Effective Atomic Charges Obtained via the EEM Method

		value						
term	parameter	BB	NN	HH	BH	NH	BN	units
dispersive	d_{ij}	15.0	15.0	15.0	15.0	15.0	15.0	----
	$s_{R,ij}$	0.8	0.8	0.784	0.784	0.784	0.8	----
	r_{ij}^{eff}	3.786	3.365	2.798	3.292	3.082	3.576	Å
	$C_{6,ij}$	1007.322	300.433	50.870	241.686	120.589	490.681	kcal · Å^6/mol
taper	$R_{\mathrm{cut},ij}$	16.0	16.0	16.0	16.0	16.0	16.0	Å
repulsive	α_{ij}	7.5	8.0	9.0	9.0	9.0	8.0	----
	β_{ij}	3.10	3.33	2.70	2.80	2.70	3.12	Å
	γ_{ij}	1.6	1.2	20.0	20.0	20.0	1.6	Å
	ε_{ij}	0.46	0.21	0.31	0.31	0.25	0.20	kcal/mol
	C_{ij}	0.45	0.66	0.13	0.13	0.13	0.10	kcal/mol
electrostatic	κ	14.4	14.4	14.4	14.4	14.4	14.4	eV · Å
	λ_{ii}	0.70	0.69	0.80	0.75	0.74	0.69	Å^{-1}
EEM	χ_i^*	10.0	11.4	10.2	----	----	----	eV
	η_i^*	6.7020	7.0000	7.0327	----	----	----	eV

distances between atomic centers i and j, respectively. The latter is defined as the shortest distance between atom j on one graphene layer and the surface normal at atom i residing on an adjacent graphene layer. With appropriate empirical parametrization, the KC potential was shown to treat accurately both interlayer binding and sliding energy variations in graphitic systems.[41] Recently, the KC functional form was adapted to treat the heterogeneous junction of graphene and hexagonal boron nitride (*h*-BN), using empirical parameter fitting.[45,46]

In order to extend the scope of the KC approach to new layered material junctions, where empirical reference data are scarce or even completely lacking, the parameter fitting procedure requires reliable reference data based on accurate computational methodologies. To this end, we recently presented a modified anisotropic ILP expression that consists of three interaction terms:[47,48] short-range repulsion, long-range attraction, and electrostatic interactions, as described in detail below.

For homogeneous *h*-BN junctions our original ILP parametrization involved fitting against Tkatchenko-Scheffler van der Waals (TS-vdW) corrected DFT reference calculations of finite dimer systems.[47,49,50] While being state-of-the-art at the time, this procedure neglects many-body dispersion (MBD) effects. An efficient and accurate scheme that takes MBD effects into account has been developed since.[51−54] As with the TS-vdW approach,[55] within the MBD approach, the problem of obtaining an accurate description of both geometry and electronic structure in weakly bound systems is decoupled. For each system, a standard DFT calculation using an exchange-correlation density functional approximation that provides a reliable description of the intralayer structure and electronic properties is performed. An MBD correction is then employed to remedy the insufficient long-range correlation description provided by standard DFT exchange-correlation functionals. This procedure typically yields CCSD(T) quality results.[48,53] Within the MBD approach, one first evaluates the TS-vdW C_6 coefficients and atomic polarizabilities by normalizing their free-atom values using their effective atomic Hirshfeld volume in the molecular or solid state environment.[56,57] Then, the atomic response functions are mapped onto a set of quantum harmonic oscillators that are coupled through dipole−dipole interactions to obtain self-consistent screened polarizabilities. The latter are used to calculate the correlation energy of the interacting oscillator model system, within the random-phase approximation.

For bulk graphite and *h*-BN, Gao and Tkatchenko have shown that MBD effects reduce binding energies by nearly a factor of 2, as compared to pairwise correction schemes, with a smaller but still noticeable effect on the interplanar distances.[58] Therefore, it is imperative to revise the ILP parametrization so as to reflect advances in the underlying first-principles theory, on which it is based. Recently, we used a range-separated version of the MBD scheme[53] to parametrize an ILP for heterogeneous graphene/*h*-BN junctions.[48] In order to provide a consistent description for homogeneous *h*-BN structures, in the

DOI: 10.1021/acs.jpcc.7b07091
J. Phys. Chem. C 2017, 121, 22826−22835

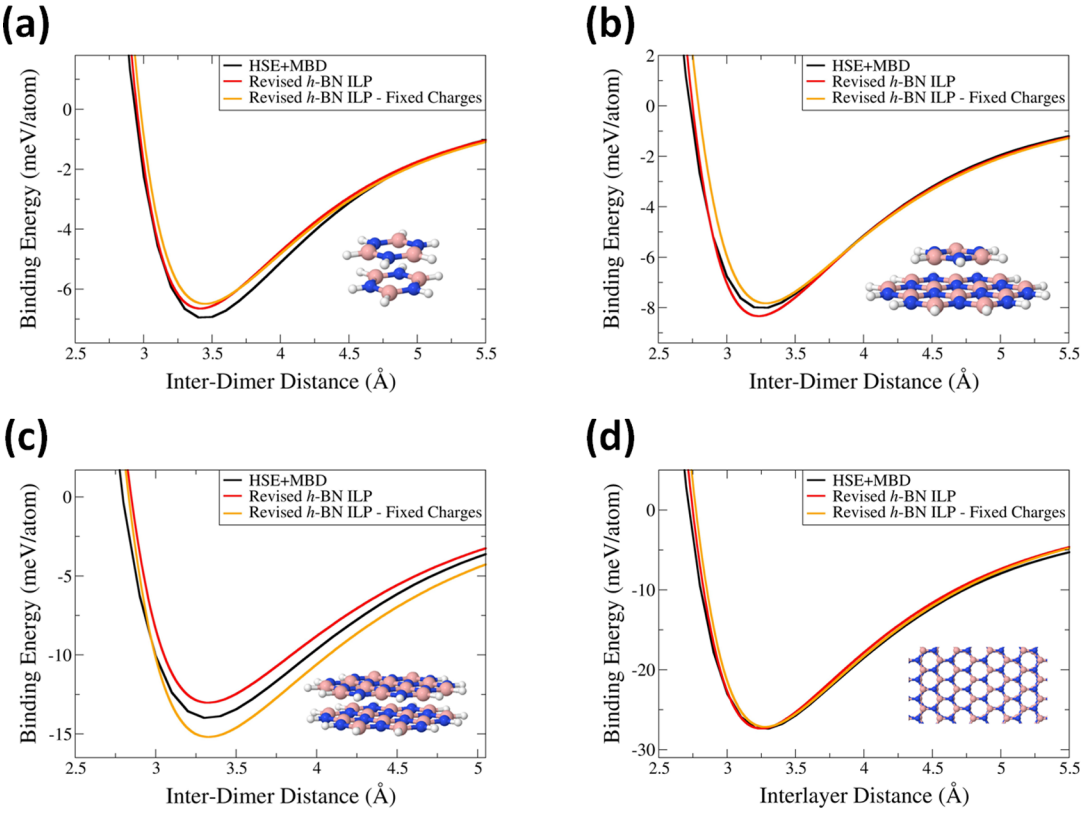

Figure 2. Binding energy curves of (a) the borazine dimer; (b) the borazine/HBNC system; (c) the HBNC dimer; and (d) a periodic *h*-BN bilayer, all calculated using the revised *h*-BN ILP with varying (red) and fixed (orange) partial charges, compared to the reference HSE+MBD results (black). The energy axis origin of each curve in panels (a)−(c) is set as the energy of the corresponding dimer at a separation of 100 Å. For the periodic bilayer system (panel (d)) the energy axis origin is calculated as twice the energy of a single *h*-BN layer.

present study we reparametrize our original *h*-BN ILP against MBD corrected reference data. Furthermore, while the KC-ILP already provides a good description of the interlayer interactions in homogeneous graphene junctions, for full compatibility with our other parametrizations we offer a complementary parametrization of our ILP term for homogeneous graphitic systems. We find that the simple pairwise ILP expression has sufficient parametric flexibility to capture the main many-body dispersion effects also for the homogeneous systems considered herein.

REFERENCE DFT CALCULATIONS

We adopt the procedure used in ref 48, where the ILP was parametrized for the heterogeneous graphene/*h*-BN junction. Four *h*-BN systems are considered: (i) the borazine dimer; (ii) borazine on hexaborazino-coronene (the BN analogue of coronene, with the chemical formula $B_{12}N_{12}H_{12}$, denoted herein as HBNC); (iii) the HBNC dimer; and (iv) a periodic *h*-BN bilayer. Correspondingly, for graphene we consider (i) the benzene dimer; (ii) benzene on coronene; (iii) the coronene dimer; and (iv) a periodic graphene bilayer.

The isolated monomers of graphene and *h*-BN were first optimized using the screened-exchange hybrid functional of Heyd, Scuseria, and Ernzerhof (HSE)[59−62] and the split-valence double-ζ 6-31G** Gaussian basis-set,[63] as implemented in the GAUSSIAN suite of programs.[64] The various dimer systems were then formed by placing pairs of monomers at their respective optimal stacking mode (AA′ for *h*-BN and AB for graphene) and interdimer distance (see Supporting Information for dimer coordinates and insets in Tables 2 and 5 below for visualization). This was followed by binding and sliding energy calculations performed by rigidly shifting the monomers with respect to each other vertically and laterally, respectively. In these calculations, we used the MBD corrected HSE functional, as implemented in the FHI-AIMS code,[65] with the tier-2 basis-set,[66] using tight convergence settings (see the Supporting Information of ref 48 for more details). Basis-set superposition errors at the equilibrium interdimer distance with this basis were previously estimated to be on the order of 0.16 meV/atom for heterogeneous graphene/*h*-BN system and 0.5 meV/atom for homogeneous *h*-BN dimers and are therefore neglected throughout the current parametrization procedure.[47,48,55,67]

To demonstrate the importance of including MBD effects in our reference calculations, we compare in Figure 1 the dimer binding-energy curves of ref 47 obtained using the pairwise TS-vdW approach applied to the B3LYP[68] hybrid density functional and the MBD correction scheme applied to the HSE functional. For completeness, we also present results obtained at the HSE+TS-vdW level of theory using the same basis-set and convergence criteria. Within the TS-vdW scheme, the onset of the pairwise correction is explicitly determined according to the amount of long-range interactions accounted for in the underlying exchange-correlation density functional approximation.[57] Hence, the difference between the B3LYP +TS-vdW and HSE+TS-vdW binding energy curves is reduced with increasing system size. On the contrary, MBD effects become more significant in larger systems. For the HBNC dimer the difference in binding energies obtained using the B3LYP+TS-vdW and HSE+TS-vdW density functionals is

DOI: 10.1021/acs.jpcc.7b07091
J. Phys. Chem. C 2017, 121, 22826−22835

Table 2. Binding Energies (BE) and Equilibrium Distances (D_{eq}) for All Finite and Periodic *h*-BN Systems Studied in Figure 2, as Obtained Using the HSE+MBD Method and the Revised *h*-BN ILP Developed in This Work[a]

Structure	Borazine dimer (D_{3d}) 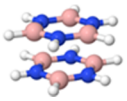		Borazine on HBNC (C_{3v}) 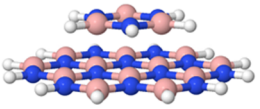	
	BE (meV/atom)	**D_{eq} (Å)**	**BE (meV/atom)**	**D_{eq} (Å)**
HSE+MBD	-6.95	3.40	-8.00	3.30
ILP	-6.65	3.41	-8.33	3.23
ILP – fixed charges	-6.49	3.45	-7.83	3.28
Structure	HBNC dimer (D_{3d}) 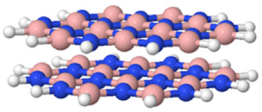		Periodic *h*-BN bilayer (D_{3d}) 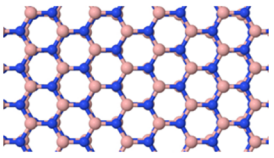	
	BE (meV/atom)	**D_{eq} (Å)**	**BE (meV/atom)**	**D_{eq} (Å)**
HSE+MBD	-13.98	3.30	-27.37	3.30
ILP	-13.02	3.32	-27.35	3.25
ILP – fixed charges	-15.18	3.33	-27.14	3.28

[a]For each system, results from both the EEM approach and the fixed-charge approach are presented. Point group symmetries of each dimer are provided in parentheses near the dimer name.

Table 3. List of ILP Parameter Values for Homogeneous *h*-BN Based Systems, Fitted Against MBD-Corrected DFT Reference Data, Using Fixed Effective Atomic Charges

		value						
term	parameter	BB	NN	HH	BH	NH	BN	units
dispersive	d_{ij}	15.0	15.0	15.0	15.0	15.0	15.0	----
	$s_{R,ij}$	0.8	0.8	0.784	0.784	0.784	0.8	----
	r_{ij}^{eff}	3.786	3.365	2.798	3.292	3.082	3.576	Å
	$C_{6,ij}$	1037.322	310.433	37.870	185.686	90.589	516.681	kcal · Å^6/mol
taper	$R_{cut,ij}$	16.0	16.0	16.0	16.0	16.0	16.0	Å
repulsive	α_{ij}	8.0	8.0	9.0	9.0	9.0	7.5	----
	β_{ij}	3.10	3.34	2.70	2.80	2.70	3.17	Å
	γ_{ij}	1.6	1.2	20.0	20.0	20.0	1.8	Å
	ϵ_{ij}	0.46	0.21	0.31	0.31	0.25	0.20	kcal/mol
	C_{ij}	0.45	0.68	0.13	0.13	0.13	0.13	kcal/mol
electrostatic	κ	14.4	14.4	14.4	14.4	14.4	14.4	eV · Å
	λ_{ij}	0.70	0.69	0.80	0.75	0.74	0.69	Å^{-1}
	q_i	0.42	−0.42	0	----	----	----	|e|

merely 0.09 meV/atom, whereas the difference between the HSE+TS-vdW and HSE+MBD binding energies is as large as 4.77 meV/atom. The latter is at least an order of magnitude above the estimated numerical accuracy of our reference calculations,[67] clearly justifying the need for reparametrization of the *h*-BN ILP.

STRUCTURE OF THE INTERLAYER POTENTIAL

Short-Range Repulsion. To describe short-range repulsion we use a screened KC-type anisotropic repulsion term of the form:

$$V_{Rep}(r_{ij}, \rho_{ij}) = \mathrm{Tap}(r_{ij}) \times e^{\alpha_{ij}\left(1-\frac{r_{ij}}{\beta_{ij}}\right)}\left[\varepsilon_{ij} + C_{ij}\left(e^{-\left(\frac{\rho_{ij}}{\gamma_{ij}}\right)^2} + e^{-\left(\frac{\rho_{ji}}{\gamma_{ij}}\right)^2}\right)\right] \quad (2)$$

where the polynomials multiplying the anisotropic Gaussian repulsion terms have been omitted and a long-range taper cutoff function of the form $\mathrm{Tap}(r_{ij}) = 20(r_{ij}/R_{cut,ij})^7 - 70(r_{ij}/R_{cut,ij})^6 + 84(r_{ij}/R_{cut,ij})^5 - 35(r_{ij}/R_{cut,ij})^4 + 1$, which provides a continuous

DOI: 10.1021/acs.jpcc.7b07091
J. Phys. Chem. C 2017, 121, 22826−22835

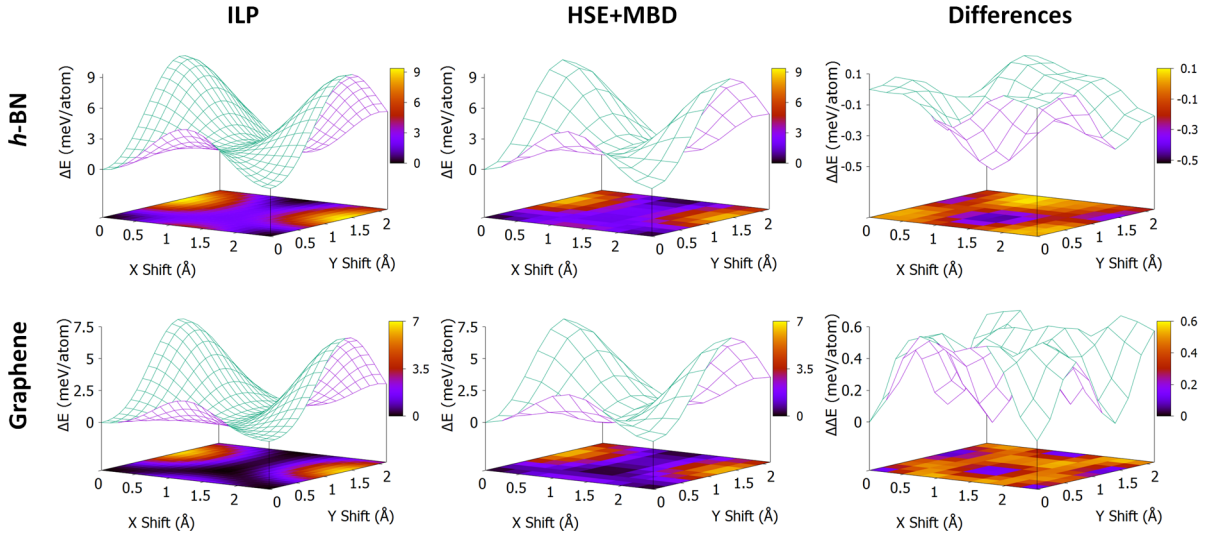

Figure 3. Sliding energy landscape of the periodic *h*-BN (upper panels) and graphene (lower panels) bilayers calculated for rigid layers laterally shifted at a fixed interlayer distance of 3.3 and 3.4 Å, respectively, using the ILP with fixed charges (left column) and HSE+MBD (middle column). The differences between the sliding energy surfaces calculated using the reference HSE+MBD data and the ILP results are presented in the right column. The energy axis origin is set to the energy of the optimally stacked configuration for each system.

Table 4. List of ILP Parameter Values for Homogeneous Graphene-Based Systems, Fitted Against MBD-Corrected DFT Reference Data

		value			
term	parameter	CC	HH	CH	units
dispersive	d_{ij}	15.0	15.0	15.0	----
	$s_{R,ij}$	0.704	0.784	0.784	----
	r_{ij}^{eff}	3.586	2.798	3.197	Å
	$C_{6,ij}$	522.915	37.870	131.989	kcal · Å^6/mol
taper	$R_{\mathrm{cut},ij}$	16.0	16.0	16.0	Å
repulsive	α_{ij}	9.2	9.0	9.0	----
	β_{ij}	3.22	2.70	2.80	Å
	γ_{ij}	1.2	20.0	20.0	Å
	ε_{ij}	0.01	0.31	0.31	kcal/mol
	C_{ij}	0.80	0.13	0.13	kcal/mol
electrostatic	q_i	0	0	----	|e|

cutoff (up to third derivative) for interatomic separations larger than $R_{\mathrm{cut},ij}$, is used to dampen the repulsion term at large distances. These modifications simplify the FF expressions and reduce the computational burden, while providing a satisfactory description of the interlayer interactions.[47,48] The parameters ε_{ij} and C_{ij} are constants that set the energy scales associated with the isotropic and anisotropic repulsion, respectively, β_{ij} and γ_{ij} set the corresponding interaction ranges, and α_{ij} is a parameter that sets the steepness of the isotropic repulsion function.

Long-Range Attraction. We adopt the screened Lennard-Jones long-range attraction term of the Tkatchenko-Scheffler (TS) correction scheme,[56] in the form

$$V_{\mathrm{Att}}(r_{ij}) = \mathrm{Tap}(r_{ij}) \times \left\{ -\left[1 + \mathrm{e}^{-d_{ij}[(r_{ij}/(S_{R,ij}\cdot r_{ij}^{\mathrm{eff}}))-1]}\right]^{-1} \cdot \frac{C_{6,ij}}{r_{ij}^{6}} \right\} \tag{3}$$

Here, r_{ij}^{eff} is the sum of effective equilibrium vdW atomic radii of atoms i and j that reside on different layers, $C_{6,ij}$ is the pairwise dispersion coefficient of the two atoms in the solid-state environment, and d_{ij} and $S_{\mathrm{R},ij}$ are unitless parameters defining the steepness and onset of the short-range Fermi–Dirac type damping function.[69] As in the repulsive term discussed above, we implement the long-range taper damping in order to reduce the computational burden. We note that the specific functional form appearing in eq 3 is chosen as it allows us to evaluate some of the parameters directly from the first-principles calculations.

Electrostatic Interaction. In cases where atoms residing on the interacting layers bear sizable effective charges, electrostatic contributions should be taken into account. To this end, we utilize the formalism implemented in the ReaxFF scheme.[70,71] Within this approach, a shielded Coulomb potential term of the form

$$V_{\mathrm{Coul}}(r_{ij}) = \mathrm{Tap}(r_{ij}) \times [23.0609 \cdot \kappa q_i q_j / \sqrt[3]{r_{ij}^3 + (1/\lambda_{ij})^3}\,] \tag{4}$$

is used. Here, κ is Coulomb's constant, q_i and q_j are the effective charges of atoms i and j that reside on different layers (given in units of the absolute value of the electron charge), the factor 23.0609 kcal/(mol eV) converts the units of energy from eV to kcal/mol, and $\lambda_{ij} = \sqrt{\lambda_{ii}\lambda_{jj}}$ is a shielding parameter that eliminates the short-range singularity of the classical monopolar electrostatic interaction expression. This shielding takes effect in regions where Pauli repulsions between overlapping electron clouds dominate the interlayer potential and hence has only a minor influence on the results. Again, we use a taper damping function to avoid the computational burden involved in the calculation of long-range electrostatic interactions. For periodic systems, this should be done with care, as some of the lattice sums may become conditionally convergent.[72] In such cases, alternative approaches such as the Ewald summation technique should be considered.[73,74]

Most often, the effective ionic charges can be treated as constant values throughout the simulation. Nevertheless, in order to provide a general description, we calculate them dynamically using the electronegativity equalization method (EEM).[70,75−77] This method relies on a principle formulated by Sanderson, stating that upon molecular or solid formation the electronegativities of the constituent atoms equalize to

DOI: 10.1021/acs.jpcc.7b07091
J. Phys. Chem. C 2017, 121, 22826−22835

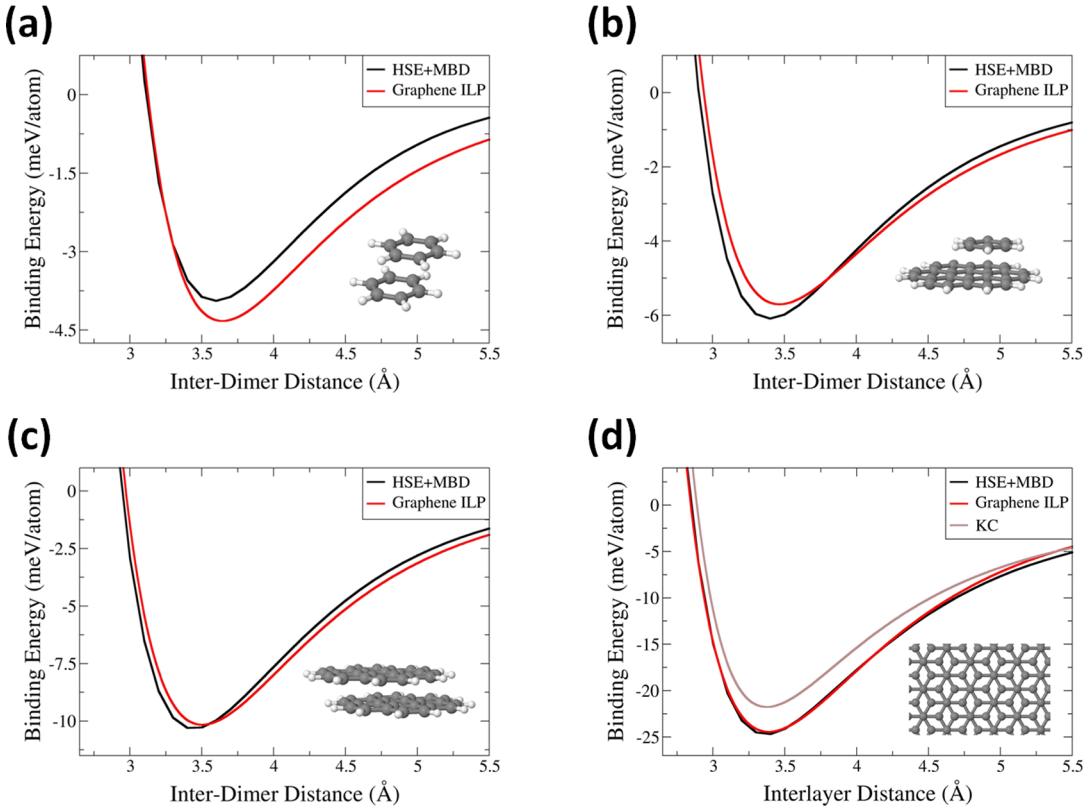

Figure 4. Binding energy curves of (a) the benzene dimer; (b) the benzene/coronene system; (c) the coronene dimer; and (d) a periodic graphene bilayer, all calculated using the graphene ILP (red) and compared to the reference HSE+MBD results (black). For further comparison, the KC binding energy curve of the periodic bilayer system (brown) is given in panel (d). The energy axis origin of each curve in panels (a)−(c) is set as the energy of the corresponding dimer at a separation of 100 Å. For the periodic bilayer system (panel (d)) the energy axis origin is calculated as twice the energy of a single graphene layer.

yield a global electronegativity of the whole system.[78,79] Hence, the electronegativity of a given atom within the molecular environment (χ_i) is written in terms of the corresponding isolated atom electronegativity[80] (χ_i^0) and hardness[81] (η_i^0) as $\chi_i = (\chi_i^0 + \Delta\chi_i) + 2(\eta_i^0 + \Delta\eta_i)q_i + \sum_{j\neq i} \kappa q_j / \sqrt[3]{r_{ij}^3 + (1/\lambda_{ij})^3}$. Here, $\Delta\chi_i$ and $\Delta\eta_i$ represent the electronegativity and hardness variations due to the embedding molecular or solid environment, and the last term incorporates the electrostatic potential induced by all other atoms in the system. The effective atomic charges can be obtained by enforcing the guiding principle that within the molecular or solid environment all atomic electronegativities should be equal to the equilibrated molecular electronegativity $\chi_{i=1\cdots N} = \chi_{eq}$. To this end, the matrix eq 5 is solved, where the isolated atomic electronegativities and hardnesses, χ_i^0 and η_i^0, their corresponding molecular environment variations, $\Delta\chi_i$ and $\Delta\eta_i$, the shielding factors, λ_{ij}, and the total charge, Q, should be provided as input. The latter is dictated by the modeled system, while the former can be parametrized as described below.

$$\begin{pmatrix} 2(\eta_1^0+\Delta\eta_1) & \kappa/\sqrt[3]{r_{12}^3+(1/\lambda_{12})^3} & \cdots & \kappa/\sqrt[3]{r_{1N}^3+(1/\lambda_{1N})^3} & -1 \\ \kappa/\sqrt[3]{r_{21}^3+(1/\lambda_{21})^3} & 2(\eta_2^0+\Delta\eta_2) & \cdots & \kappa/\sqrt[3]{r_{2N}^3+(1/\lambda_{2N})^3} & -1 \\ \vdots & \vdots & \ddots & \vdots & \vdots \\ \kappa/\sqrt[3]{r_{N1}^3+(1/\lambda_{N1})^3} & \kappa/\sqrt[3]{r_{N2}^3+(1/\lambda_{N2})^3} & \cdots & 2(\eta_N^0+\Delta\eta_N) & -1 \\ 1 & 1 & \cdots & 1 & 0 \end{pmatrix} \begin{pmatrix} q_1 \\ q_2 \\ \vdots \\ q_N \\ \chi_{eq} \end{pmatrix} = - \begin{pmatrix} \chi_1^0+\Delta\chi_1 \\ \chi_2^0+\Delta\chi_2 \\ \vdots \\ \chi_N^0+\Delta\chi_N \\ -Q \end{pmatrix} \quad (5)$$

PARAMETER FITTING

All ILP parameters discussed above were fit, within reasonable physical bounds, to obtain good agreement with the reference binding and sliding energy curves. Specifically, for the long-range attraction term the parameter values obtained via the TS-vdW scheme were used as a starting point for further refinement. The parametrization is intentionally biased toward better agreement with the reference data of extended systems, where MBD effects become more significant. These systems are harder to treat using first-principles methods. Therefore, they require the use of approximate approaches that provide a good balance between accuracy and computational efficiency, such as the developed ILP.

Table 1 provides the full set of ILP parameter values suggested for homogeneous *h*-BN based systems. The resulting binding energy curves of all *h*-BN based dimer models considered in this work are compared to the reference HSE+MBD data in Figure 2. It is readily observed that the revised ILP (red) reproduces the reference binding energy curves (black) well. The largest deviations in the calculated binding energy and equilibrium distance are 0.96 meV/atom and 0.07 Å (see Table 2), obtained for the HBNC dimer and Borazine on HBNC systems, respectively. Notably, for the periodic bilayer system the agreement between the ILP and reference data is within 0.02 meV/atom near the equilibrium interlayer distance. A comparison with the original *h*-BN ILP parametrization, performed against TS-vdW corrected B3LYP reference data,[47] demonstrates that the revised version typically yields smaller binding energies and somewhat increased equilibrium interdimer distances (see Supporting Information), consistent with the corresponding reference first-principles calculations (see Figure 1).

DOI: 10.1021/acs.jpcc.7b07091
J. Phys. Chem. C 2017, 121, 22826−22835

Table 5. Binding Energies (BE) and Equilibrium Distances (D_{eq}) for All Finite and Periodic Graphene Systems Studied in Figure 4, as Obtained Using the HSE+MBD Approach and the Graphene ILP Developed in This Work[a]

Structure	Benzene dimer (C_{2h}) 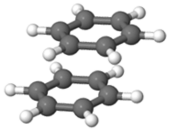		Benzene on Coronene (C_s) 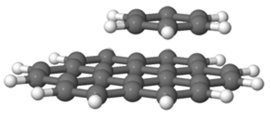	
	BE (meV/atom)	D_{eq} (Å)	BE (meV/atom)	D_{eq} (Å)
HSE+MBD	-3.94	3.60	-6.09	3.40
ILP	-4.33	3.64	-5.70	3.47
Structure	**Coronene dimer (C_{2h})** 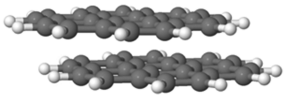		**Periodic graphene bilayer (D_{3d})** 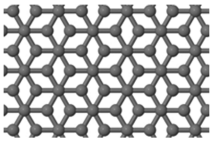	
	BE (meV/atom)	D_{eq} (Å)	BE (meV/atom)	D_{eq} (Å)
HSE+MBD	-10.30	3.40	-24.67	3.40
ILP	-10.16	3.51	-24.44	3.38

[a]Point group symmetries of each dimer are provided in parentheses near the dimer name.

Importantly, the calculated partial charges on the boron and nitrogen atoms are found to be quite insensitive to the relative positioning of the monomers within a given dimer system. Therefore, in order to reduce the computational burden, one can usually avoid the EEM calculation by using fixed partial charges. To obtain a good fit with the reference data, this requires some modification of the parameters in the non-electrostatic terms to compensate for the fixing of the charge. Table 3 provides the full set of ILP parameters to be used when fixed partial charges are implied. The corresponding binding-energy curves (orange lines in Figure 2) show good agreement with the reference data, with maximal binding-energy and equilibrium interdimer distance deviations of 1.2 meV/atom and 0.05 Å obtained for the HCBN dimer and the Borazine dimer systems, respectively (see Table 2). Considerably smaller binding-energy (0.23 meV/atom) and equilibrium interdimer distance (0.02 Å) deviations are obtained for the periodic bilayer system.

An important feature of the developed ILP is its ability to simultaneously capture both the interlayer binding and sliding energy landscapes. To verify this, we show in Figure 3 the sliding energy landscape of the periodic *h*-BN bilayer (upper panels), calculated using the ILP with the fixed-charge parametrization of Table 3 (upper left panel), compared to the reference sliding energy landscape obtained using HSE+MBD (upper middle panel). Excellent quantitative agreement between the two surfaces is obtained, with maximal deviations of 0.52 meV/atom (upper right panel). This clearly demonstrates that the anisotropic nature of the ILP is sufficient to provide a good description of both binding and sliding physics of *h*-BN based systems even in the presence of many-body dispersion effects.

As mentioned above, for completeness we offer in Table 4 the recommended ILP parameters for graphitic systems. This is not intended to replace the KC formalism but rather to provide a uniform platform when performing calculations on different layered materials. The resulting ILP binding energy curves (red) are compared to the HSE+MBD reference data (black) in Figure 4. Here too, good agreement between the ILP and the reference data is obtained, with maximal binding-energy deviation of 0.39 meV/atom for the benzene dimer and benzene-on-coronene systems, and maximal interdimer equilibrium distance deviation of 0.11 Å obtained for the coronene dimer system (see Table 5), with considerably smaller deviations (0.23 meV/atom and 0.02 Å, respectively) obtained for the periodic bilayer system. For comparison, the KC binding energy curve of the periodic system (brown) is provided in Figure 4d. As can be seen, the KC parametrization, fit to experimental reference data, predicts a very similar interlayer distance (3.37 Å) with a somewhat smaller (−21.75 meV/atom) binding energy.

To verify that the ILP parametrization for graphene can also capture the interlayer sliding physics, we also show in Figure 3 the sliding energy landscape of the periodic graphene bilayer (lower panels) calculated using the ILP (lower left panel) with the parametrization of Table 4 compared to the reference sliding energy landscape obtained using HSE+MBD (lower middle panel). Here too, excellent quantitative agreement between the two surfaces is obtained, with maximal deviations as small as 0.59 meV/atom (lower right panel).

SUMMARY AND CONCLUSIONS

We presented a reparametrization of the interlayer potential for hexagonal boron nitride that considers many-body dispersion effects. The new set of parameters is calibrated against binding and sliding energy surfaces calculated for a set of dimer systems using MBD-corrected density functional theory calcula-

DOI: 10.1021/acs.jpcc.7b07091
J. Phys. Chem. C 2017, 121, 22826−22835

tions based on the screened-exchange-correlation HSE density functional. A complementary set of HSE+MBD calibrated ILP parameters was also provided for graphitic systems, for transferability purposes. For all systems considered, the ILP was found to yield good agreement with the new reference data, with binding-energies that can be nearly twice as small as those obtained via the previous TS-vdW reference calculations. Combined with our previous ILP parametrization for the heterogeneous graphene/*h*-BN junction, these allow for flexible and internally consistent simulations of the mechanical, tribological, dynamical, and heat transport properties of both homogeneous and heterogeneous layered structures based on graphene and *h*-BN.

■ ASSOCIATED CONTENT

Supporting Information

The Supporting Information is available free of charge on the ACS Publications website at DOI: 10.1021/acs.jpcc.7b07091.

Comparison of the reference binding-energy curves calculated for the various *h*-BN dimers at the HSE+MBD and B3LYP+TS-vdW levels of theory and the corresponding ILP results (PDF)

Coordinates of the various dimers considered, placed at their HSE+MBD equilibrium distance, as obtained for the optimal stacking mode of the corresponding infinite bilayer system (XLSX)

■ AUTHOR INFORMATION

Corresponding Author

*E-mail: odedhod@tau.ac.il.

ORCID

Oded Hod: 0000-0003-3790-8613

Author Contributions

#Tal Maaravi and Itai Leven contributed equally to this work.

Notes

The authors declare no competing financial interest.

■ ACKNOWLEDGMENTS

Work at TAU was supported by the Israel Science Foundation, the Lise-Meitner Minerva Center for Computational Quantum Chemistry and the Center for Nanoscience and Nanotechnology at Tel-Aviv University. Work at Weizmann was supported by the historical generosity of the Perlman family. The authors would like to thank Prof. Alexandre Tkatchenko and Dr. Vivekanand V. Gobre for helpful discussions.

■ REFERENCES

(1) Novoselov, K. S.; Geim, A. K.; Morozov, S. V.; Jiang, D.; Zhang, Y.; Dubonos, S. V.; Grigorieva, I. V.; Firsov, A. A. Electric Field Effect in Atomically Thin Carbon Films. *Science* **2004**, *306*, 666−669.

(2) Novoselov, K. S.; Jiang, D.; Schedin, F.; Booth, T. J.; Khotkevich, V. V.; Morozov, S. V.; Geim, A. K. Two-Dimensional Atomic Crystals. *Proc. Natl. Acad. Sci. U. S. A.* **2005**, *102*, 10451−10453.

(3) Geim, A. K.; Novoselov, K. S. The Rise of Graphene. *Nat. Mater.* **2007**, *6*, 183−191.

(4) Li, D.; Kaner, R. B. Graphene-Based Materials. *Science* **2008**, *320*, 1170−1171.

(5) Geim, A. K. Graphene: Status and Prospects. *Science* **2009**, *324*, 1530−1534.

(6) Rao, C. N. R.; Sood, A. K.; Subrahmanyam, K. S.; Govindaraj, A. Graphene: The New Two-Dimensional Nanomaterial. *Angew. Chem., Int. Ed.* **2009**, *48*, 7752−7777.

(7) Geim, A. K.; Grigorieva, I. V. Van der Waals Heterostructures. *Nature* **2013**, *499*, 419−425.

(8) Wang, H.; Liu, F.; Fu, W.; Fang, Z.; Zhou, W.; Liu, Z. Two-Dimensional Heterostructures: Fabrication, Characterization, and Application. *Nanoscale* **2014**, *6*, 12250−12272.

(9) Heine, T. Transition Metal Chalcogenides: Ultrathin Inorganic Materials with Tunable Electronic Properties. *Acc. Chem. Res.* **2015**, *48*, 65−72.

(10) Li, X.; Zhu, H. Two-Dimensional MoS2: Properties, Preparation, and Applications. *J. Materiomics* **2015**, *1*, 33−44.

(11) Das, S.; Robinson, J. A.; Dubey, M.; Terrones, H.; Terrones, M. Beyond Graphene: Progress in Novel Two-Dimensional Materials and van der Waals Solids. *Annu. Rev. Mater. Res.* **2015**, *45*, 1−27.

(12) Novoselov, K. S.; Mishchenko, A.; Carvalho, A.; Castro Neto, A. H. 2D Materials and van der Waals Heterostructures. *Science* **2016**, *353*, aac9439.

(13) Koren, E.; Leven, I.; Lörtscher, E.; Knoll, A.; Hod, O.; Duerig, U. Coherent Commensurate Electronic States at the Interface Between Misoriented Graphene Layers. *Nat. Nanotechnol.* **2016**, *11*, 752−757.

(14) Barone, V.; Hod, O.; Peralta, J. E.; Scuseria, G. E. Accurate Prediction of the Electronic Properties of Low-Dimensional Graphene Derivatives Using a Screened Hybrid Density Functional. *Acc. Chem. Res.* **2011**, *44*, 269−279.

(15) Rappe, A. K.; Casewit, C. J.; Colwell, K. S.; Goddard, W. A.; Skiff, W. M. UFF, a Full Periodic Table Force Field for Molecular Mechanics and Molecular Dynamics Simulations. *J. Am. Chem. Soc.* **1992**, *114*, 10024−10035.

(16) Al-Jishi, R.; Dresselhaus, G. Lattice-Dynamical Model for Graphite. *Phys. Rev. B: Condens. Matter Mater. Phys.* **1982**, *26*, 4514−4522.

(17) Tersoff, J. Empirical Interatomic Potential for Carbon, with Applications to Amorphous Carbon. *Phys. Rev. Lett.* **1988**, *61*, 2879−2882.

(18) Brenner, D. W. Empirical Potential for Hydrocarbons for Use in Simulating the Chemical Vapor Deposition of Diamond Films. *Phys. Rev. B: Condens. Matter Mater. Phys.* **1990**, *42*, 9458−9471.

(19) Brenner, D. W. Tersoff-Type Potentials for Carbon, Hydrogen, and Oxygen. *MRS Online Proc. Libr.* **1988**, *141*, 59−64.

(20) Stuart, S. J.; Tutein, A. B.; Harrison, J. A. A Reactive Potential for Hydrocarbons with Intermolecular Interactions. *J. Chem. Phys.* **2000**, *112*, 6472−6486.

(21) Brenner, D. W.; Shenderova, O. A.; Harrison, J. A.; Stuart, S. J.; Ni, B.; Sinnott, S. B. A Second-Generation Reactive Empirical Bond Order (REBO) Potential Energy Expression for Hydrocarbons. *J. Phys.: Condens. Matter* **2002**, *14*, 783.

(22) Los, J. H.; Fasolino, A. Intrinsic Long-Range Bond-Order Potential for Carbon: Performance in Monte Carlo Simulations of Graphitization. *Phys. Rev. B: Condens. Matter Mater. Phys.* **2003**, *68*, 024107.

(23) Ghiringhelli, L. M.; Los, J. H.; Meijer, E. J.; Fasolino, A.; Frenkel, D. Modeling the Phase Diagram of Carbon. *Phys. Rev. Lett.* **2005**, *94*, 145701.

(24) Los, J. H.; Ghiringhelli, L. M.; Meijer, E. J.; Fasolino, A. Improved Long-Range Reactive Bond-Order Potential for Carbon. I. Construction. *Phys. Rev. B: Condens. Matter Mater. Phys.* **2005**, *72*, 214102.

(25) Ghiringhelli, L. M.; Valeriani, C.; Los, J. H.; Meijer, E. J.; Fasolino, A.; Frenkel, D. State-of-the-Art Models for the Phase Diagram of Carbon and Diamond Nucleation. *Mol. Phys.* **2008**, *106*, 2011−2038.

(26) Perebeinos, V.; Tersoff, J. Valence Force Model for Phonons in Graphene and Carbon Nanotubes. *Phys. Rev. B: Condens. Matter Mater. Phys.* **2009**, *79*, 241409.

(27) Lindsay, L.; Broido, D. A. Optimized Tersoff and Brenner Empirical Potential Parameters for Lattice Dynamics and Phonon Thermal Transport in Carbon Nanotubes and Graphene. *Phys. Rev. B: Condens. Matter Mater. Phys.* **2010**, *81*, 205441.

(28) Jiang, J.-W. Graphene versus MoS2: A Short Review. *Front. Phys.* **2015**, *10*, 287−302.

(29) O'Connor, T. C.; Andzelm, J.; Robbins, M. O. AIREBO-M: A Reactive Model for Hydrocarbons at Extreme Pressures. *J. Chem. Phys.* **2015**, *142*, 024903.
(30) Sevik, C.; Kinaci, A.; Haskins, J. B.; Çağın, T. Characterization of Thermal Transport in Low-Dimensional Boron Nitride Nanostructures. *Phys. Rev. B: Condens. Matter Mater. Phys.* **2011**, *84*, 085409.
(31) Wakabayashi, N.; Smith, H. G.; Nicklow, R. M. Lattice Dynamics of Hexagonal MoS2 Studied by Neutron Scattering. *Phys. Rev. B* **1975**, *12*, 659−663.
(32) Jiménez Sandoval, S.; Yang, D.; Frindt, R. F.; Irwin, J. C. Raman Study and Lattice Dynamics of Single Molecular Layers of MoS2. *Phys. Rev. B: Condens. Matter Mater. Phys.* **1991**, *44*, 3955−3962.
(33) Brunier, T. M.; Drew, M. G. B.; Mitchell, P. C. H. Molecular Mechanics Studies of Molybdenum Disulphide Catalysts Parameterisation of Molybdenum and Sulphur. *Mol. Simul.* **1992**, *9*, 143−159.
(34) Morita, Y.; Onodera, T.; Suzuki, A.; Sahnoun, R.; Koyama, M.; Tsuboi, H.; Hatakeyama, N.; Endou, A.; Takaba, H.; Kubo, M.; et al. Development of a New Molecular Dynamics Method for Tribochemical Reaction and its Application to Formation Dynamics of MoS2 Tribofilm. *Appl. Surf. Sci.* **2008**, *254*, 7618−7621.
(35) Liang, T.; Phillpot, S. R.; Sinnott, S. B. Parametrization of a Reactive Many-Body Potential for Mo-S Systems. *Phys. Rev. B: Condens. Matter Mater. Phys.* **2009**, *79*, 245110.
(36) Varshney, V.; Patnaik, S. S.; Muratore, C.; Roy, A. K.; Voevodin, A. A.; Farmer, B. L. MD Simulations of Molybdenum Disulphide (MoS2): Force-Field Parameterization and Thermal Transport Behavior. *Comput. Mater. Sci.* **2010**, *48*, 101−108.
(37) Jiang, J.-W.; Park, H. S.; Rabczuk, T. Molecular Dynamics Simulations of Single-Layer Molybdenum Disulphide (MoS2): Stillinger-Weber Parametrization, Mechanical Properties, and Thermal Conductivity. *J. Appl. Phys.* **2013**, *114*, 064307.
(38) Nicolini, P.; Polcar, T. A Comparison of Empirical Potentials for Sliding Simulations of MoS2. *Comput. Mater. Sci.* **2016**, *115*, 158−169.
(39) Karssemeijer, L. J.; Fasolino, A. Phonons of Graphene and Graphitic Materials Derived from the Empirical Potential LCBOPII. *Surf. Sci.* **2011**, *605*, 1611−1615.
(40) Ghiringhelli, L. M.; Los, J. H.; Fasolino, A.; Meijer, E. J. Improved Long-Range Reactive Bond-Order Potential for Carbon. II. Molecular Simulation of Liquid Carbon. *Phys. Rev. B: Condens. Matter Mater. Phys.* **2005**, *72*, 214103.
(41) Reguzzoni, M.; Fasolino, A.; Molinari, E.; Righi, M. C. Potential Energy Surface for Graphene on Graphene: Ab Initio Derivation, Analytical Description, and Microscopic Interpretation. *Phys. Rev. B: Condens. Matter Mater. Phys.* **2012**, *86*, 245434.
(42) Jiang, J.-W.; Park, H. S. A Gaussian Treatment for the Friction Issue of Lennard-Jones Potential in Layered Materials: Application to Friction Between Graphene, MoS2, and Black Phosphorus. *J. Appl. Phys.* **2015**, *117*, 124304.
(43) Kolmogorov, A. N.; Crespi, V. H. Smoothest Bearings: Interlayer Sliding in Multiwalled Carbon Nanotubes. *Phys. Rev. Lett.* **2000**, *85*, 4727−4730.
(44) Kolmogorov, A. N.; Crespi, V. H. Registry-Dependent Interlayer Potential for Graphitic Systems. *Phys. Rev. B: Condens. Matter Mater. Phys.* **2005**, *71*, 235415.
(45) van Wijk, M. M.; Schuring, A.; Katsnelson, M. I.; Fasolino, A. Moiré Patterns as a Probe of Interplanar Interactions for Graphene on h-BN. *Phys. Rev. Lett.* **2014**, *113*, 135504.
(46) Woods, C. R.; Withers, F.; Zhu, M. J.; Cao, Y.; Yu, G.; Kozikov, A.; Ben Shalom, M.; Morozov, S. V.; van Wijk, M. M.; Fasolino, A.; et al. Macroscopic Self-Reorientation of Interacting Two-Dimensional Crystals. *Nat. Commun.* **2016**, *7*, 10800.
(47) Leven, I.; Azuri, I.; Kronik, L.; Hod, O. Inter-Layer Potential for Hexagonal Boron Nitride. *J. Chem. Phys.* **2014**, *140*, 104106.
(48) Leven, I.; Maaravi, T.; Azuri, I.; Kronik, L.; Hod, O. Interlayer Potential for Graphene/h-BN Heterostructures. *J. Chem. Theory Comput.* **2016**, *12*, 2896−2905.
(49) Leven, I.; Guerra, R.; Vanossi, A.; Tosatti, E.; Hod, O. Multiwalled Nanotube Faceting Unravelled. *Nat. Nanotechnol.* **2016**, *11*, 1082−1086.
(50) Oz, I.; Leven, I.; Itkin, Y.; Buchwalter, A.; Akulov, K.; Hod, O. Nanotube Motion on Layered Materials: A Registry Perspective. *J. Phys. Chem. C* **2016**, *120*, 4466−4470.
(51) Tkatchenko, A.; DiStasio, R. A.; Car, R.; Scheffler, M. Accurate and Efficient Method for Many-Body van der Waals Interactions. *Phys. Rev. Lett.* **2012**, *108*, 236402.
(52) DiStasio, R. A.; von Lilienfeld, O. A.; Tkatchenko, A. Collective Many-Body Van der Waals Interactions in Molecular Systems. *Proc. Natl. Acad. Sci. U. S. A.* **2012**, *109*, 14791−14795.
(53) Ambrosetti, A.; Reilly, A. M.; DiStasio, R. A.; Tkatchenko, A. Long-Range Correlation Energy Calculated from Coupled Atomic Response Functions. *J. Chem. Phys.* **2014**, *140*, 18A508.
(54) Kronik, L.; Tkatchenko, A. Understanding Molecular Crystals with Dispersion-Inclusive Density Functional Theory: Pairwise Corrections and Beyond. *Acc. Chem. Res.* **2014**, *47*, 3208−3216.
(55) Marom, N.; Tkatchenko, A.; Scheffler, M.; Kronik, L. Describing Both Dispersion Interactions and Electronic Structure Using Density Functional Theory: The Case of Metal−Phthalocyanine Dimers. *J. Chem. Theory Comput.* **2010**, *6*, 81−90.
(56) Tkatchenko, A.; Scheffler, M. Accurate Molecular Van Der Waals Interactions from Ground-State Electron Density and Free-Atom Reference Data. *Phys. Rev. Lett.* **2009**, *102*, 073005.
(57) Marom, N.; Tkatchenko, A.; Rossi, M.; Gobre, V. V.; Hod, O.; Scheffler, M.; Kronik, L. Dispersion Interactions with Density-Functional Theory: Benchmarking Semiempirical and Interatomic Pairwise Corrected Density Functionals. *J. Chem. Theory Comput.* **2011**, *7*, 3944−3951.
(58) Gao, W.; Tkatchenko, A. Sliding Mechanisms in Multilayered Hexagonal Boron Nitride and Graphene: The Effects of Directionality, Thickness, and Sliding Constraints. *Phys. Rev. Lett.* **2015**, *114*, 096101.
(59) Heyd, J.; Scuseria, G. E.; Ernzerhof, M. Hybrid Functionals Based on a Screened Coulomb Potential. *J. Chem. Phys.* **2003**, *118*, 8207−8215.
(60) Heyd, J.; Scuseria, G. E. Assessment and Validation of a Screened Coulomb Hybrid Density Functional. *J. Chem. Phys.* **2004**, *120*, 7274−7280.
(61) Heyd, J.; Scuseria, G. E. Efficient Hybrid Density Functional Calculations in Solids: Assessment of the Heyd−Scuseria−Ernzerhof Screened Coulomb Hybrid Functional. *J. Chem. Phys.* **2004**, *121*, 1187−1192.
(62) Heyd, J.; Scuseria, G. E.; Ernzerhof, M. Erratum: "Hybrid Functionals Based on a Screened Coulomb Potential" [J. Chem. Phys.118, 8207 (2003)]. *J. Chem. Phys.* **2006**, *124*, 219906.
(63) Hariharan, P. C.; Pople, J. A. The Influence of Polarization Functions on Molecular Orbital Hydrogenation Energies. *Theor. Chim. Acta* **1973**, *28*, 213−222.
(64) Frisch, M. J.; Trucks, G. W.; Schlegel, H. B.; Scuseria, G. E.; Robb, M. A.; Cheeseman, J. R.; Scalmani, G.; Barone, V.; Mennucci, B.; Petersson, G. A., et al. *Gaussian 09*, Revision A.02; Wallingford, CT, 2009.
(65) Blum, V.; Gehrke, R.; Hanke, F.; Havu, P.; Havu, V.; Ren, X.; Reuter, K.; Scheffler, M. Ab Initio Molecular Simulations with Numeric Atom-Centered Orbitals. *Comput. Phys. Commun.* **2009**, *180*, 2175−2196.
(66) Havu, V.; Blum, V.; Havu, P.; Scheffler, M. Efficient O(N) Integration for All-Electron Electronic Structure Calculation Using Numeric Basis Functions. *J. Comput. Phys.* **2009**, *228*, 8367−8379.
(67) Marom, N.; Bernstein, J.; Garel, J.; Tkatchenko, A.; Joselevich, E.; Kronik, L.; Hod, O. Stacking and Registry Effects in Layered Materials: The Case of Hexagonal Boron Nitride. *Phys. Rev. Lett.* **2010**, *105*, 046801.
(68) Becke, A. D. Density-Functional Thermochemistry. III. The Role of Exact Exchange. *J. Chem. Phys.* **1993**, *98*, 5648−5652.
(69) Note that since $S_{R,ij}$ multiplies r_{ij}^{eff} and they are both fitting parameters of the ILP any set of their values that produces the same multiplication is equivalent. The final choice of relative values of these parameter is thus chosen to be within reasonable physical bounds.

DOI: 10.1021/acs.jpcc.7b07091
J. Phys. Chem. C 2017, 121, 22826−22835

(70) van Duin, A. C. T.; Dasgupta, S.; Lorant, F.; Goddard, W. A. ReaxFF: A Reactive Force Field for Hydrocarbons. *J. Phys. Chem. A* **2001**, *105*, 9396−9409.
(71) Weismiller, M. R.; Duin, A. C. T. v.; Lee, J.; Yetter, R. A. ReaxFF Reactive Force Field Development and Applications for Molecular Dynamics Simulations of Ammonia Borane Dehydrogenation and Combustion. *J. Phys. Chem. A* **2010**, *114*, 5485−5492.
(72) Hod, O. Graphite and Hexagonal Boron-Nitride Have the Same Interlayer Distance. Why? *J. Chem. Theory Comput.* **2012**, *8*, 1360−1369.
(73) Ewald, P. P. Die Berechnung Optischer und Elektrostatischer Gitterpotentiale. *Ann. Phys.* **1921**, *369*, 253−287.
(74) Toukmaji, A. Y.; Board, J. A. Ewald Summation Techniques in Perspective: a Survey. *Comput. Phys. Commun.* **1996**, *95*, 73−92.
(75) Mortier, W. J.; Ghosh, S. K.; Shankar, S. Electronegativity-Equalization Method for the Calculation of Atomic Charges in Molecules. *J. Am. Chem. Soc.* **1986**, *108*, 4315−4320.
(76) Njo, S. L.; Fan, J.; van de Graaf, B. Extending and Simplifying the Electronegativity Equalization Method. *J. Mol. Catal. A: Chem.* **1998**, *134*, 79−88.
(77) Bultinck, P.; Langenaeker, W.; Lahorte, P.; De Proft, F.; Geerlings, P.; Waroquier, M.; Tollenaere, J. P. The Electronegativity Equalization Method I: Parametrization and Validation for Atomic Charge Calculations. *J. Phys. Chem. A* **2002**, *106*, 7887−7894.
(78) Sanderson, R. T. An Interpretation of Bond Lengths and a Classification of Bonds. *Science* **1951**, *114*, 670−672.
(79) Sanderson, R. T.: *Polar Covalence*; Academic Press: New York, 1983.
(80) Parr, R. G.; Donnelly, R. A.; Levy, M.; Palke, W. E. Electronegativity: The Density Functional Viewpoint. *J. Chem. Phys.* **1978**, *68*, 3801−3807.
(81) Parr, R. G.; Pearson, R. G. Absolute Hardness: Companion Parameter to Absolute Electronegativity. *J. Am. Chem. Soc.* **1983**, *105*, 7512−7516.

DOI: 10.1021/acs.jpcc.7b07091
J. Phys. Chem. C 2017, 121, 22826−22835